Available online at www.sciencedirect.com
ScienceDirect
Estuarine, Coastal and Shelf Science 78 (2008) 190–202
ESTUARINE COASTAL AND SHELF SCIENCE
www.elsevier.com/locate/ecss

A numerical study of tidal asymmetry in Okatee Creek, South Carolina

Haosheng Huang [a,*], Changsheng Chen [a], Jackson O. Blanton [b], Francisco A. Andrade [c]

[a] School for Marine Science and Technology, University of Massachusetts Dartmouth, New Bedford, MA 02744, USA
[b] Skidaway Institute of Oceanography, Savannah, GA 31411, USA
[c] Guia Marine Laboratory, Faculty of Sciences of Lisbon University, Lisbon, Portugal

Received 30 April 2006; accepted 19 November 2007
Available online 23 December 2007

Abstract

The Okatee River, South Carolina is characterized by a narrow tidal channel and an extensive area of intertidal salt marshes. Current measurements in the upstream portion Okatee Creek show that tidal flow features an asymmetric pattern: ebb current is stronger than flood current. The ebb dominance is mainly caused by deformation of the dominant astronomical tidal constituent M_2. An unstructured grid, finite volume coastal ocean model (FVCOM) with wet-dry point treatment method is applied to examine physical mechanisms of M_4 overtide generation. Model experiments show that mean absolute amplitude and phase errors are 3.1 cm and 1.7° for M_2 elevation, 2.4 cm s^{-1} and 0.8° for M_2 current major axis, 2.1 cm and 1.8° for M_4 elevation, and 2.1 cm s^{-1} and 24.6° for M_4 current major axis. The overall pattern of tidal asymmetry is qualitatively reproduced. Various sensitivity experiments suggest that the generation of M_4 overtide is a result of nonlinear interaction of tidal currents with irregular creek geometry and bottom topography. Consistent with the classical view, the large volume of intertidal water storage is the major reason for ebb dominance in the creek. However, the zero-inertia assumption (i.e., negligible advective terms) is probably not valid for the entire tidal cycle. Besides the pressure gradient force and the bottom friction force, terms related to lateral shear of the along-estuary velocity (i.e., advective inertia and horizontal eddy viscosity) may also contribute in horizontal momentum balance. Exclusion of the flooding-draining processes over the intertidal zone will severely underestimate tidal currents in the river channel and make the tidal asymmetry less prominent. Published by Elsevier Ltd.

Keywords: tidal asymmetry; ebb dominance; intertidal salt marsh; FVCOM; numerical simulation; Okatee Creek

1. Introduction

Astronomical tidal waves (e.g., M_2) that propagate into coastal shelves and enter bays and estuaries can generate shallow water and compound constituents (e.g., M_4, M_6, and others). Nonlinear physical processes are responsible for the production of overtides. Due to superposition of these constituents, tidal current and water level are distorted from their sinusoidal forms, which give rise to tidal asymmetry. The case that the duration of falling tide is longer is referred to as flood dominance because the maximum velocity is greater in flood than in ebb (assuming that current is purely tide induced). The opposite case is referred to as ebb dominance. Tidal asymmetry plays an important role in sediment transport pattern and channel morphology (Dronkers, 1986; Aldridge, 1997), as well as in lateral transfer of salt (Blanton and Andrade, 2001) in various tidal embayments and estuaries.

Tidal dynamics in a channel with variable width and depth has been studied for one-dimensional (1-D) flow. Four principal sources of nonlinearity are identified in the generation of overtides (Parker, 1991), i.e., advective inertia, quadratic friction, time-varying channel depth in the friction term, and time-varying channel depth coupled with time-varying estuary width in the continuity equation. Limiting case studies, defined by relative intensity of friction versus advective inertia in the momentum equation and by the role of channel convergence in the mass balance, have been carried out to explore contributing factors in tidal asymmetry. In weakly dissipative estuaries, tidal propagation is essentially a weakly nonlinear phenomenon. Tidal wave speed and the rate of spatial growth or decay of tidal amplitude depend strongly on the degree of

* Corresponding author. Department of Oceanography and Coastal Sciences, Louisiana State University, Baton Rouge, LA 70803, USA.
E-mail address: hhuang7@lsu.edu (H. Huang).

0272-7714/$ - see front matter Published by Elsevier Ltd.
doi:10.1016/j.ecss.2007.11.027

channel convergence (Jay, 1991). Overtides are generated in a cascade process such that higher harmonics have decreasing amplitude (Lanzoni and Seminara, 1998). When channel convergence is moderate or strong, weakly dissipative tidal channels turn out to be ebb dominated due to the nonlinearity arising from advective inertia (Lanzoni and Seminara, 1998).

The weak dissipation assumption is rarely realistic in tide-dominant estuaries, especially for those with large tidal amplitude to depth ratio. LeBlond (1978) suggested that in shallow estuaries the dominant momentum balance is between the pressure gradient force and the bottom friction force. As a result of the negligible role of horizontal advection, tidal propagation in shallow river channels behaves as a diffusive process rather than a hyperbolic wave (LeBlond, 1978; Friedrichs and Madsen, 1992). The nonlinear friction term causes a larger drag effect at low water than at high water. In turn, the high water crest catches up with the low water trough and the rising tide is of short duration, yielding flood dominance (Dronkers, 1986; Friedrichs and Aubrey, 1994).

A large area of tidal flats or marshes may significantly alter the dynamics of a tidal creek. In particular, it is shown that, owing to the effect of intertidal water storage, the flood dominance typical of strongly dissipative estuaries may change to be ebb dominance (Speer et al., 1991; Shetye and Gouveia, 1992). Two parameters are important in determining the tidal asymmetry in such an estuary: the ratio of tidal amplitude to mean water depth and the ratio of intertidal storage volume to that of main river channel (Speer and Aubrey, 1985; Friedrichs and Aubrey, 1988).

The Okatee/Colleton River, a branch of the Broad River along South Carolina coast, is a typical tide-controlled shallow estuary that is characterized by extensive intertidal salt marshes, tidal creeks, small islands, and isolated barriers (Fig. 1). M_2 is the dominant tidal constituent in this estuary, which accounts for more than 85% of the water surface variation. The tidal range is over 3 m during spring tide. Mean water depth in the main water channel varies from 15 m near the river mouth to 2–4 m in headwater tidal creeks (i.e., Okatee Creek and Malind Creek; Fig. 1). Thus, the ratio of tidal amplitude to mean water depth is about 0.2 in the downstream region and close to 1 in the upstream tidal creeks. There is a vast area of salt marsh zone in this estuary, which is depicted by the 2-m water elevation line in Fig. 1. In the Okatee/Colleton River the area of intertidal salt marshes is comparable to the open water area of main river channel. Further upstream the salt marsh area becomes much larger than that of main water channel.

Time series observation of axial current and water level at several stations in Okatee Creek shows that the tidal current is ebb dominant (South Carolina Sea Grant Consortium, 2005). The most conspicuous asymmetry is the difference between the maximum ebb and flood current. At station D (see Fig. 1 for its location) the maximum ebb current is about 60 cm s^{-1}, almost twice the value of maximum flood current (Fig. 2a). The tidal asymmetry is also apparent in the shape of the current time series which is not sinusoidal. The maximum ebb current occurs more or less at the mid-point between the time of high-water-slack (HWS) and low-water-slack

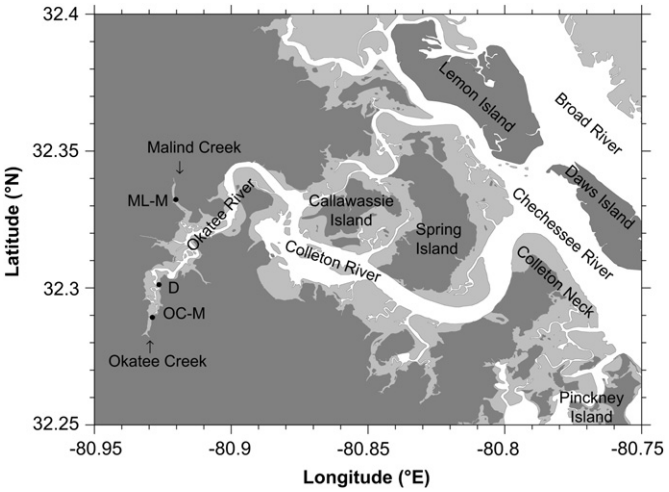

Fig. 1. Geographic location of the Okatee/Colleton Rivers. The white-filled area is the river channel, which is below the mean low water (MLW), and the gray-filled area is the 2-m intertidal salt marsh zone. The boundary between the dark gray and the gray area is the 2-m water elevation line. The filled dots (D, OC-M, and ML-M) are locations of water elevation measurements and current meter moorings. Okatee Creek is the headwater tidal creek of the Okatee River, while Malind Creek is a side channel of the Okatee River.

(LWS), while the maximum flood current occurs much closer to the time of LWS. This feature is more obviously seen at station OC-M, where both maximum currents occur closer to the LWS time (Fig. 2b).

Many investigations have been performed to study the controlling factors of overtide generation in coastal embayments and estuaries. However, few studies have utilized a fully three-dimensional (3-D) primitive equation numerical model. A 1-D analytic or numerical model, though a useful tool in understanding overtide dynamics, is unable to yield a detailed model-data comparison due to its inability to incorporate realistic estuarine geometry. In the Okatee/Colleton River, large salt marsh area, small barrier islands, sinuosity of the river channel and its various side channels are all sources of local overtide generation. In this study, a 3-D, finite-volume coastal ocean model (FVCOM) is applied to simulate the tidal creek–intertidal salt marsh environment and to explore the factors controlling asymmetric tidal field.

In the interest of conceptual simplicity, only the astronomical tidal constituent M_2 and its harmonic M_4 are considered in the numerical experiments. Such an approach is justified because observations show that M_2 is the dominant tidal constituent and M_4 is the dominant shallow water constituent in the study area. So presumably the effect of other tidal constituents on tidal deformation is minor.

This study demonstrates that FVCOM is capable of yielding a qualitatively accurate simulation of asymmetrical tidal fields in Okatee Creek. The various sensitivity experiments conducted confirm the classical view that ebb dominance is a result of nonlinear interaction of tidal currents with intertidal storage volume. However, analysis of the momentum balance in the solution shows that the pressure gradient term and the bottom friction term are not always dominant in the model. The paper is organized as follows. Section 2 presents

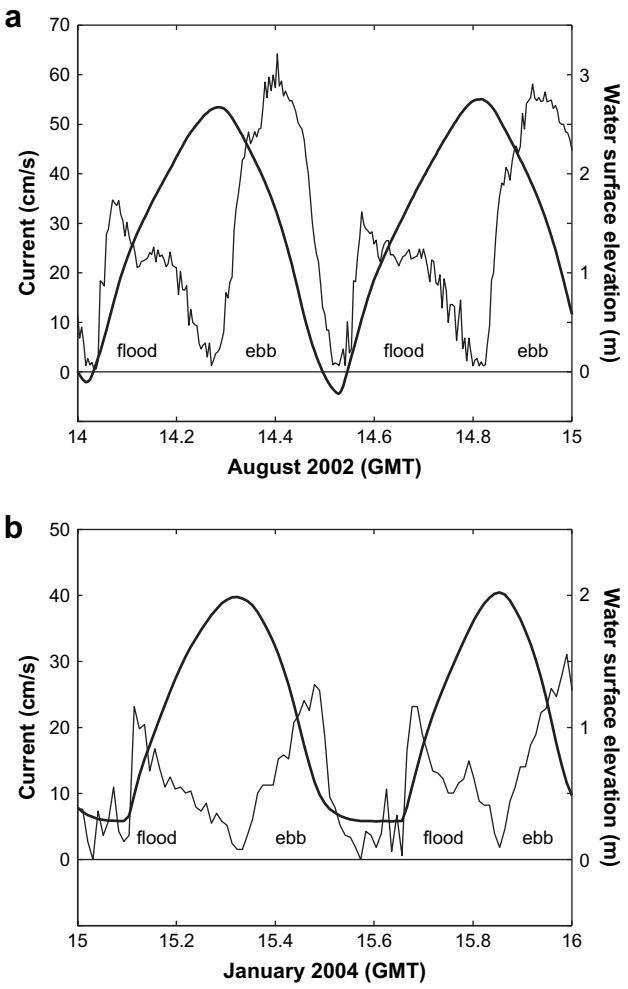

Fig. 2. Observed time series of axial tidal current (thin line) versus water surface elevation (thick line) at (a) station D, and (b) station OC-M in Okatee Creek. See Fig. 1 for station locations.

descriptions of the numerical model and experimental setup. Section 3 describes available observational data that are used to make model verification. Analysis of tidal current calculations in the base experiment and in various sensitivity experiments are given in Sections 4 and 5, respectively. Section 6 gives a discussion of controlling factors of tidal asymmetry in Okatee Creek. Finally, Section 7 offers a summary of the results.

2. Description of the numerical model and its configuration

The finite-volume coastal ocean model (FVCOM) is a newly developed 3-D free surface primitive equation model (Chen et al., 2003). FVCOM uses an unstructured triangular grid in the horizontal to better match the sinuous estuarine channels and land boundaries. Validation experiments indicate that accuracy of geometric fitting is critical in numerical simulations of tidal amplitude and phase (Chen et al., 2007). A terrain following sigma coordinate is employed in the vertical. FVCOM uses the modified Mellor and Yamada level 2.5 (MY-2.5) turbulent closure scheme for vertical mixing (Mellor and Yamada, 1982; Galperin et al., 1988) and Smagorinsky eddy parameterization for horizontal dissipation and diffusion (Smagorinsky, 1963). For a detailed description of FVCOM discrete equations and various boundary conditions, readers are referred to Chen et al. (2003, 2004). Here we just reiterate that a conventional quadratic bottom friction formulation is used in FVCOM, as we will test the influence of this nonlinear term on the M_4 generation process.

A wet/dry point treatment method has been incorporated into FVCOM. During ebb tide once the vertical column thickness is less than 5 cm, the model flow is extremely viscous. The cell is therefore designated as a dry cell and its velocity is set to zero. When the water level rises during the flood phase, a dry cell can become wet as soon as its thickness exceeds 5 cm and its velocity and elevation are computed from discrete equations. This method has been used in a Georgia estuary to simulate the periodic flooding and draining processes over intertidal zones (Zheng et al., 2003).

An FVCOM application that covers the entire Okatee/Colleton estuary has been run before (Chen et al., submitted for Publication). The horizontal resolution of that model is ~250 m in the main water channel and ~35 m in the upstream Okatee Creek (Fig. 3). From now on, we will refer to the result from this model as the large domain model result. The large domain FVCOM provides a reasonable simulation of surface elevation and current in the main channel of the Okatee/Collecton estuary, but the amplitude of major overtide constituent M_4 is significantly underestimated (Chen et al., submitted for Publication). We believe the failure of the large domain model to adequately reproduce the M_4 is in large part due to the coarse horizontal resolution and over-smoothed bathymetry used in that simulation, particularly near the headwater tidal creeks.

In 2001, the Okatee River was surveyed during the flooding tidal phase using airborne infra-red vertical photography mosaics (South Carolina Sea Grant Consortium, 2005; Blanton

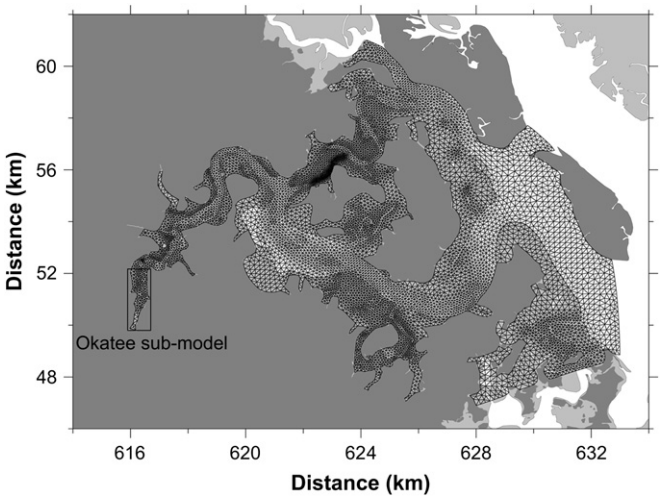

Fig. 3. The unstructured triangular grid configured for the FVCOM Okatee/Colleton River model (called the large domain model in this study). The horizontal resolution is 250 m in outer area close to the open boundary and 35 m in the upstream tidal creeks. The box depicts computational domain of the subdomain model for Okatee Creek.

et al., 2006). A 1 × 1 m resolution digital elevation map (DEM) in the intertidal zone was constructed after the survey for the Okatee and Malind Creeks. The DEM provides detailed topographic data (Fig. 4b) and allows a unique opportunity to examine overtide generation mechanisms in the narrow tidal creeks. A sub-domain model in Okatee Creek is thus constructed (Figs. 3 and 4a), in which the horizontal resolution is 10–15 m in the main creek channel and 20–40 m on the surrounding salt marshes. There are 7 uniform sigma levels in the vertical.

The Okatee Creek sub-model is driven by M_2 and M_4 elevations at the northern open boundary, which are obtained from observations at a nearby station. To avoid numerical instability caused by a sharp change in initial conditions (i.e., null velocity and surface elevation everywhere), the tidal forcing is ramped up from zero to its full value over two M_2 cycles. Freshwater is injected into the model domain at the upstream end of the creek (southmost part of the model domain). The discharge rate of 0.01 $m^3\ s^{-1}$ used in the base experiment is determined, using the trial and error method, by matching model predicted harmonic constants with observational ones. To focus on the process study of shallow water tide generation mechanism, the density field is constant in all experiments. This assumption is justified by the small freshwater discharge rate mentioned above and by the shallowness of the headwater tidal creek in which strong tidal mixing will quickly make the water column vertically uniform. Field observations showed that a seagrass canopy had an overall damping effect on flow above (Nepf and Vivoni, 2000; Verduin and Backhaus, 2000). As a zeroth-order approximation to incorporate the salt marshes into a numerical simulation, we specify a bottom drag coefficient 10 times greater in the salt marsh zone than in the main river channel.

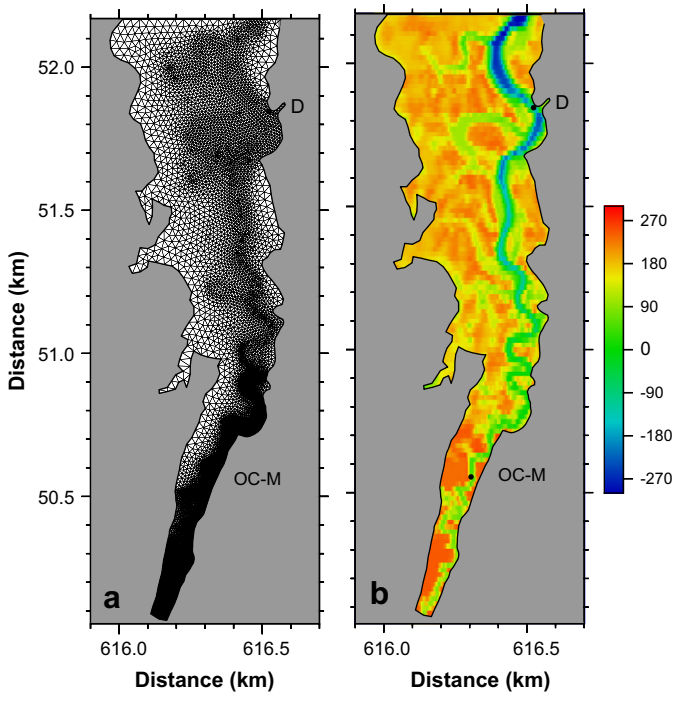

Fig. 4. (a) The unstructured triangular grid of the Okatee Creek sub-model. The horizontal resolution is about 10–15 m in the channel of the tidal creek and about 20–40 m over the intertidal salt marsh zone. (b) Bottom bathymetry (in centimeters) used in the FVCOM Okatee Creek sub-model. This bathymetry is interpolated from the 1 × 1 m digital elevation map in the intertidal zone observed in the upstream Okatee River. The filled dots are locations of station D and OC-M, respectively.

3. The tidal observation in Okatee Creek

There are two tidal observation sites, station D and OC-M (Figs. 1 and 4), along the 2 km long main channel of Okatee Creek. Station D is located in the downstream part of Okatee Creek. Subsurface pressure was measured with a Sea-Bird Electronics Model 37SM MicroCAT recorder fixed 1 m off bottom from 27 March 2001 to 11 July 2002 (South Carolina Sea Grant Consortium, 2005). An InterOcean S4 electromagnetic current meter was configured at the same site, 1 m off bottom, to measure currents from 8 August 2002 to 15 August 2002. Site OC-M is a USGS station in the upstream end of the creek. The gage height and sectionally averaged current from 1 January 2004 to 30 March 2004 were downloaded from USGS website (http://waterdata.usgs.gov/sc/nwis/uv/?site_no=02176575). The sampling interval of the MicroCAT and S4 was 10 min, and the sampling rate of the USGS measurement was 15 min.

Foreman's tidal harmonic analysis program (Pawlowicz et al., 2002) is used to calculate the amplitude and the phase from the water level elevation and the tidal current observation time series (Tables 1 and 2). The narrow creek channel confines the motion of the tidal currents to be almost rectilinear, so the minor axis of the current ellipse is much smaller than the major axis. Hence, only the major axis of the current ellipse is given in Table 2. It should be noted that the duration of current measurement at station D is short. As a result, the error in the current harmonic constants at this station is relatively large.

Tables 1 and 2 show that the observed amplitude of the M_2 tide decreases from 115.4 cm at station D to 93.6 cm at station OC-M, while its phase increases from 52.6°G to 57.1°G. The major current axis of the same constituent decreases upstream from 43.4 cm s^{-1} to 19.7 cm s^{-1} and its phase increases from 326.3°G to 343.4°G. The sharp reduction in M_2 current indicates that bottom friction exerted a large drag on the major astronomical tidal wave entering this shallow creek. As a result, shallow water constituents are generated. The observed M_4 amplitudes are 13.9 cm and 4.9 cm for station D and OC-M respectively (Table 1) while the M_4 current amplitudes are 10.2 cm s^{-1} and 3.3 cm s^{-1} (Table 2).

4. The tidal simulation in Okatee Creek

The Okatee sub-model experiment using standard model configuration as described in Section 2 is referred to as Okatee Creek Experiment 1 (OCE1). It forms the base experiment with which various sensitivity experiments, as will be discussed in Section 5, are compared. The result of OCE1 is discussed in this section.

Table 1 shows the amplitude and the phase of the M_2 and the M_4 constituents, which are extracted from model output using a least square fitting program. The harmonic constants of

Table 1
Observed and model-computed water level amplitudes and phases of M_2 and M_4 tidal constituents in Okatee Creek. Experiment OCE1 is the base experiment, which is described in detail in Section 2. The major difference between various numerical experiments and the base experiment is listed in the experiment description column. Phase angles (in degree) are referred to Greenwich mean time (GMT). The observed tidal amplitude and phase are reported with 95% of confidence interval estimates

Experiment description			M_2 tide		M_4 tide	
			Station D	Station OC-M	Station D	Station OC-M
Observed		Amplitude (cm)	115.4 (2.8)	93.6 (3.0)	13.9 (2.8)	4.9 (2.2)
		Phase (degrees)	52.6 (1.5)	57.1 (1.7)	250.6 (10.4)	166.6 (25.0)
OCE 1	Base experiment	Amplitude (cm)	113.0	97.4	14.7	1.4
		Phase (degrees)	51.4	59.3	249.7	164.1
OCE 2	No intertidal zone	Amplitude (cm)	112.9	100.1	14.5	3.4
		Phase (degrees)	51.1	54.7	250.4	65.0
OCE 3	Water depth 3 m increase	Amplitude (cm)	112.7	112.7	14.7	14.7
		Phase (degrees)	51.4	51.5	252.3	253.3
OCE 4	No nonlinear advection	Amplitude (cm)	112.9	98.0	14.7	1.2
		Phase (degrees)	51.2	57.5	249.7	119.5
OCE 5	Linear bottom friction	Amplitude (cm)	112.7	85.2	15.0	3.9
		Phase (degrees)	51.8	71.3	249.5	288.6
OCE 6	M_2 only	Amplitude (cm)	112.9	101.4	0.5	9.8
		Phase (degrees)	51.4	58.2	171.8	257.4
OCE 7	Increased river discharge	Amplitude (cm)	113.0	95.8	14.7	0.8
		Phase (degrees)	51.4	59.1	249.7	198.8
LDE	Large domain experiment	Amplitude (cm)	110.0	110.0	5.0	5.0
		Phase (degrees)	51.5	51.7	27.0	27.0

vertically averaged velocity components at corresponding model locations are presented in Table 2. As can be seen, in experiment OCE1 the mean absolute deviations of model-computed and observed amplitude and phase difference are 3.1 cm and 1.7° for M_2 elevation, 2.4 cm s^{-1} and 0.8° for M_2 current major axis, 2.1 cm and 1.8° for M_4 elevation, and 2.1 cm s^{-1} and 24.6° for M_4 current major axis. The M_2 constituent relative errors, as represented by the ratio of model-data amplitude difference to the observed amplitude, are 1.9% and 4.0% for elevation and 9.2% and 4.6% for current at station D and OC-M, respectively. Large relative errors are found for M_4 constituent, partly due to the small amplitude of the observed overtide. For example, at OC-M the M_4 elevation amplitude is off by a factor of ~3 and the averaged M_4 major axis difference is ~35%. Nevertheless, our M_4 simulation skill is about the same order as that reported in other numerical studies (e.g., Davies and Lawrence (1994) in the Irish Sea: ~5 cm and 40° for elevation RMS errors; Zheng et al. (2003) in a Georgia estuary: 1.7 cm, 23.4° for elevation RMS errors, and 6.2 cm s^{-1}, 19.8° for major axis and current phase RMS errors).

Table 2
Observed and model-computed tidal current ellipses of M_2 and M_4 constituents in Okatee Creek. Experiment OCE1 is the base experiment, which is described in detail in Section 2. The major difference between various numerical experiments and the base experiment is listed in the experiment description column. U_{major}, amplitude of the major axis; G, Greenwich phase (in degrees) of maximum current. The amplitude of the minor axis is much smaller than U_{major} and is not shown. The observed values for tidal ellipse parameters are reported with 95% of confidence interval estimates

Experiment description			M_2 tide		M_4 tide	
			Station D	Station OC-M	Station D	Station OC-M
Observed		U_{major} (cm s^{-1})	43.4 (2.6)	19.7 (2.0)	10.2 (2.5)	3.3 (0.8)
		G (degrees)	326.3 (3.3)	343.4 (5.1)	321.7 (14.3)	263.1 (15.5)
OCE 1	Base experiment	U_{major} (cm s^{-1})	39.4	20.6	7.4	4.7
		G (degrees)	326.6	344.8	295.5	240.0
OCE 2	No intertidal zone	U_{major} (cm s^{-1})	11.9	10.9	5.1	2.4
		G (degrees)	320.7	342.2	185.9	237.3
OCE 3	Water depth 3 m increase	U_{major} (cm s^{-1})	9.6	2.6	6.0	1.4
		G (degrees)	328.1	323.9	183.3	180.0
OCE 4	No nonlinear advection	U_{major} (cm s^{-1})	38.5	20.6	9.4	3.9
		G (degrees)	326.6	340.2	242.2	236.7
OCE 5	Linear bottom friction	U_{major} (cm s^{-1})	43.4	15.0	10.4	1.9
		G (degrees)	331.6	359.4	266.0	188.3
OCE 6	M_2 only	U_{major} (cm s^{-1})	39.3	20.8	10.0	3.1
		G (degrees)	324.6	340.2	203.5	121.5
OCE 7	Increased river discharge	U_{major} (cm s^{-1})	39.4	20.8	7.3	5.4
		G (degrees)	326.8	355.1	294.9	6.4
LDE	Large domain experiment	U_{major} (cm s^{-1})	13.0	3.0	1.0	1.0
		G (degrees)	327.0	335.0	306.0	8.0

Fig. 5 shows snapshots of water coverage and near-surface tidal current vectors at different phases during the M_2 tidal period. During flood tide the water intrudes and covers most of the intertidal storage region ~2 h after LWS (Fig. 5c), while during ebb tide the salt marshes are not dried until ~4 h after HWS (Fig. 5e). This indicates that the morphology in Okatee Creek is characterized by a low intertidal zone (not much higher than MLW), which tides spill into and drain out of soon after and shortly before LWS. Strong ebb and flood currents are seen to appear in the main river channel and the

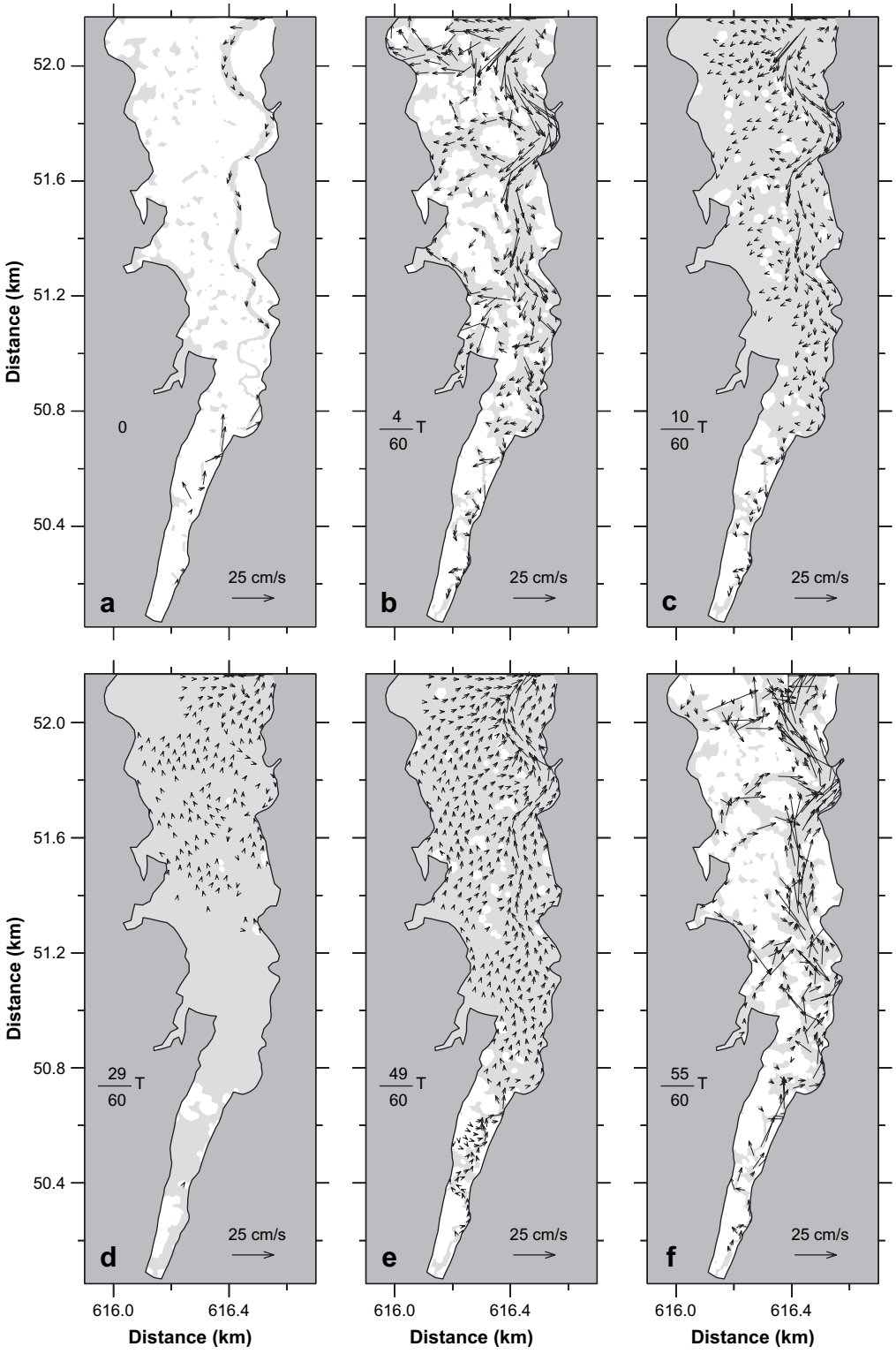

Fig. 5. FVCOM simulated flooding and draining process and current vectors in Okatee Creek for (a) low-water-slack (LWS) time, (b) 4/60 *T* after LWS, (c) 10/60 *T* after LWS, (d) 29/60 *T* after LWS, (e) 49/60 *T* after LWS, and (f) 55/60 *T* after LWS, where *T* is the period of the M_2 tidal constituent. The white-filled area is dried while the gray-filled area is submerged.

side channels when most of the intertidal area is not covered by waters (Fig. 5b,f). Hence, the maximum flood and ebb currents occur relatively close to LWS along most of the creek.

Tidal asymmetry at station D and OC-M is illustrated in Fig. 6. When compared to Fig. 2 it is seen that experiment OCE1 simulates two observed features of the tidal field. The maximum ebb current is greater than the maximum flood current as in the observations. The asymmetry is stronger at the downstream station D where the former is nearly 40% larger than the latter. The timing of the maximum ebb and flood currents are shifted closer to LWS at the upstream station OC-M. This is another aspect of the observed tidal asymmetry captured by the model, although at station D the time shift in the model is not as conspicuous as it is in the observations. We suspect that this discrepancy is caused by inaccurate bottom topography used in the model near this station and this issue will be discussed in Section 6.

Additionally, observations show that low water at station OC-M does not have a sharp end but decreases slowly until rapid rising as the flood tide begins (Fig. 2b). This indicates that water level at ebb tide is prevented from falling to the same level further downstream (such as station D) due to the existence of extensive shoals near OC-M. This phenomenon is also reflected in experiment OCE1 (Fig. 6b).

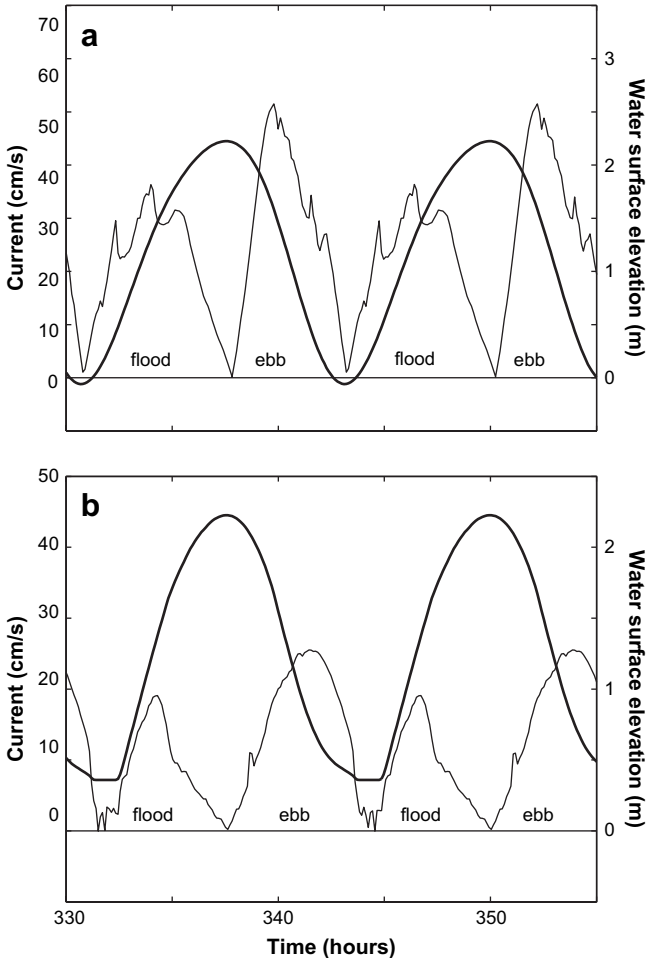

Fig. 6. FVCOM simulated time series of tidal current (thin line) versus water surface elevation (thick line) at (a) station D, and (b) station OC-M in Okatee Creek in experiment OCE1 (the base experiment).

While there are quantitative differences between observed and model-predicted tidal fields, especially for the phase of M_4 major current axis (Table 2), the similarity between qualitative patterns in observed and model-predicted tidal elevation and current (Fig. 6) gives us confidence in using the model to examine the processes influencing the M_4 tide. In the next section, various sensitivity experiments are conducted. Some possible reasons for data-model discrepancy are discussed in Section 6.

5. Numerical investigation of tidal asymmetry in Okatee Creek

In addition to experiment OCE1, seven more numerical experiments are conducted to examine the tidal processes in the Okatee Creek sub-model. Their differences from OCE1, in model geometry, boundary forcing, or bottom friction formulation, are summarized in Tables 1 and 2. The large domain experiment (LDE) result (Chen et al., submitted for Publication) is also reported for comparison.

5.1. Importance of the intertidal storage volume (OCE2 and OCE3)

According to 1-D theory (Speer and Aubrey, 1985; Friedrichs and Aubrey, 1988), two parameters that influence tidal asymmetry in embayments and estuaries are the ratio of the intertidal storage volume to that of the river channel and the ratio of the tidal amplitude to the mean water depth. To assess the importance of intertidal storage volume on the M_4 generation, the salt marsh region (the area with bathymetry above mean water depth) is removed from the computation domain (experiment OCE2). Thus the numerical grid only covers the north-southward main river channel in Okatee Creek (Fig. 4b). Omitting this intertidal volume has a very small effect on the simulated amplitude of M_2 and M_4 elevations (Table 1). However, it severely reduces both tidal currents (Table 2). For example, at station D the major axis of M_4 current is about two-thirds of that in OCE1 and it decreases to less than one-third for the M_2 constituent. Relatively large changes in phase are also noted, especially in the M_4 elevation at Station OC-M and the M_4 current at Station D. As a consequence, the asymmetric characteristic of the tidal current is far less prominent in OCE2 (Fig. 7a,b).

In OCE3, the mean water depth in the whole creek is increased 3 m uniformly while all other conditions are kept the same as in OCE1. Thus, the ratio of the tidal amplitude to the mean water depth is decreased from 0.5−1 in OCE1 to 0.2− 0.3 in OCE3. Due to increased water depth, the periodic flooding-drying process over the intertidal zone disappears. Hence, the salt marsh zone in OCE1 can no longer be regarded as an intertidal storage volume in this experiment. In Table 1 the model-predicted amplitudes of M_2 and M_4 tidal elevation have no decay between station D and OC-M, and their phases are also almost the same. This indicates that

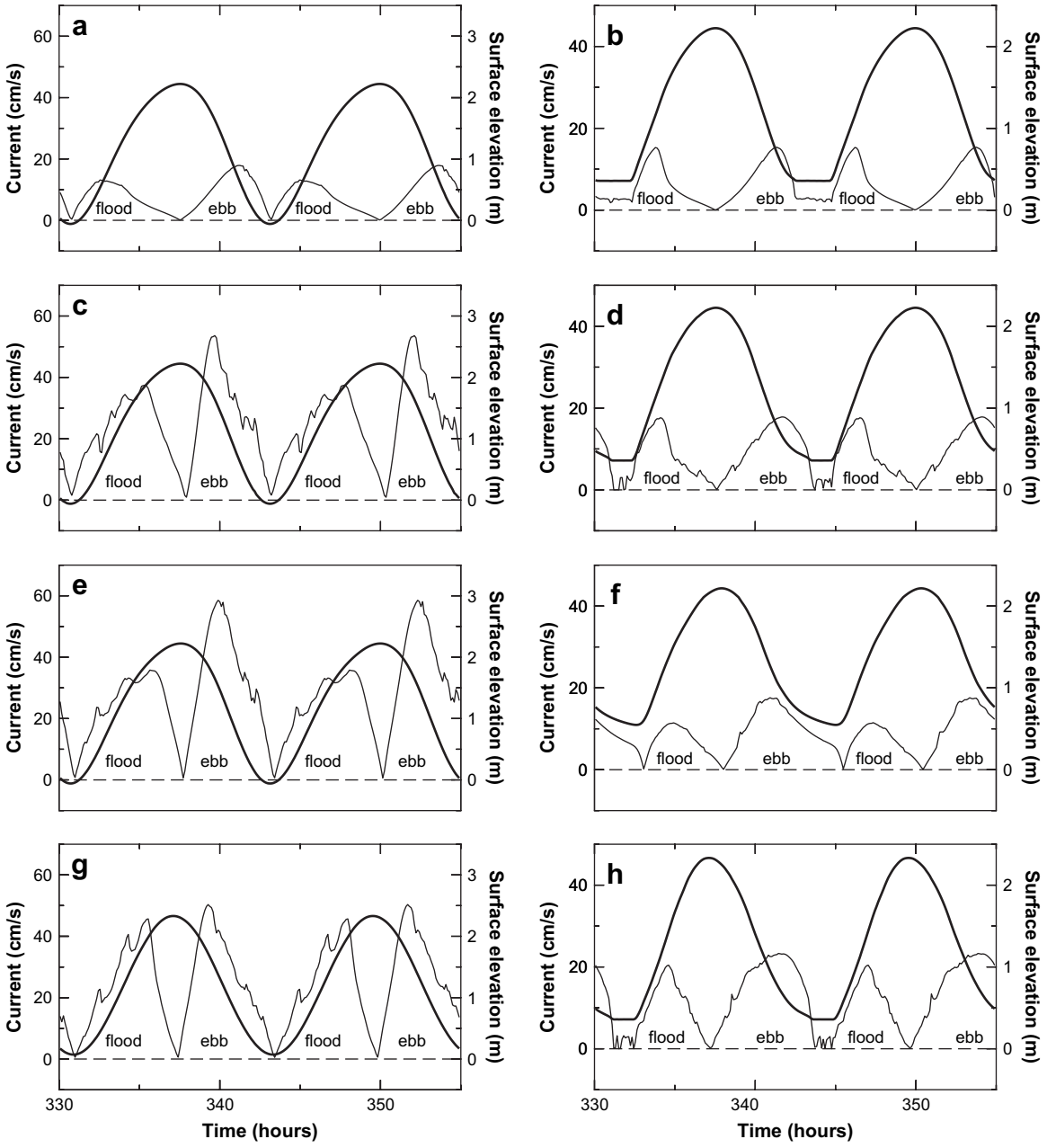

Fig. 7. FVCOM simulated time series of tidal current (thin line) and water surface elevation (thick line) in experiment OCE2 (experiment with intertidal zone removed) at station D (a) and station OC-M (b), in experiment OCE4 (experiment with nonlinear terms removed) at station D (c) and station OC-M (d), in experiment OCE5 (experiment with linear bottom friction) at station D (e) and station OC-M (f), and in experiment OCE6 (experiment with M_2 open boundary forcing only) at station D (g) and station OC-M (h).

frictional dissipation decreases due to increased water depth. The computed amplitudes of both tidal currents reduce greatly with respect to OCE1 (Table 2), which can be probably attributed to the enlarged channel cross-section due to depth increase. Similar to OCE2 the ebb dominant tidal asymmetry almost disappears in this experiment (figure not shown).

5.2. *Effect of nonlinear advection and bottom friction formulation (OCE4 and OCE5)*

In experiment OCE4, all nonlinear horizontal advection terms are neglected in the x and y momentum equations. In this simulation the M_2 elevation and the M_2 current are similar in both amplitude and phase to the predictions in experiment OCE1 (Tables 1 and 2). However, the phases of M_4 elevation at station OC-M and M_4 current at station D show differences of $\sim 45^{\circ}$G and 50°G, respectively. This results in the disappearance of ebb dominance at station OC-M (Fig. 7d). The maximum flood current also shifts closer to HWS at station D in comparison to OCE1 (Fig. 7c). This experiment suggests that the M_2 tidal dynamics in this small tidal creek can be described quite well with the linear theory but nonlinear advective terms must be taken into account in the simulation of M_4 overtide.

Experiment OCE5 examines the role of the bottom friction term. When the quadratic term used in OCE1 is replaced with a linear formulation, the maximum flood current also shifts closer to HWS at station D (Fig. 7e). Frictional effects are also significant at station OC-M where the tidal range in this experiment is about 10 cm smaller than that in OCE1, mainly due to the amplitude decrease of M_2 elevation (Fig. 7f and Table 1). As a consequence, the water shoaling process is totally different from experiment OCE1 in that no sluggish current exists near low water. Quadratic and linear formulations for bottom friction are two of the most commonly used parameterization methods in the current literature. Experiment OCE5 suggests that quadratic formulation is better than the linear one in capturing the asymmetric tidal field in this tidal creek.

5.3. Effect of the M_4 open boundary forcing (OCE6)

In this small sub-domain model, two sources contribute to the observed M_4 strength. One is the local overtide generation due to nonlinear processes. The other is M_4 generated downstream (outside sub-domain open boundary) which may affect the upstream region. To separate these two sources, the M_4 tidal forcing at the open boundary is removed (OCE6). The resulting M_2 tide does not change much in this experiment in comparison with experiment OCE1. However, the M_4 constituent is different in both tidal elevation and tidal current magnitude. At station D, the M4 elevation amplitude is small while at station OC-M it is quite large (Table 1). The major axis of M_4 current ellipse behaves to the contrary, i.e., is smaller at OC-M and greater at D with respect to OCE1 (Table 2). The larger M_4 current at station D in OCE6 does not result in stronger asymmetry in the tidal current curve (Fig. 7 g), which is probably due to the unfavorable phase relationship. Therefore, this experiment clearly illustrates that the M_4 overtide generated in the lower reach of the Okatee River plays an important role in ebb dominance in Okatee Creek and it must be imposed as a boundary condition in Okatee Creek only simulation.

5.4. Effect of the horizontal resolution (LDE)

In a shallow tidal creek with complex bathymetry such as Okatee Creek, the horizontal resolution of a numerical model limits the topographic features that can be incorporated. This, in turn, limits the accuracy of the simulated tidal asymmetry because the formation of shallow water tides depends critically on the interaction between the tides and the bottom topography. This is one of the reasons why the model-predicted major axis of the M_4 current ellipse is one order of magnitude smaller (only 1 cm s^{-1}) than the values observed in the large domain experiment LDE (Table 2). This indicates that the M_4 current is barely generated in the large domain experiment due to its low resolution of topographic features.

5.5. Effect of river discharge (OCE7)

Experiment OCE7 is run in which the river discharge rate is increased by a factor of 10 (0.1 m^3 s^{-1}). Numerical results show that it has neither much effect on the amplitudes and the phases of M_2 and M_4 elevation, nor much effect on the major axes of tidal current ellipses at station D (Tables 1 and 2). Large changes relative to OCE1 occur for the phases of M_4 elevation and current at station OC-M, which may be attributed to the increased seaward pressure gradient induced by river discharge. Results from OCE7 suggest that the relatively large phase error found in the M_4 tidal current could be related to the inaccurate estimation of river discharge rate in the model.

6. Discussion

LeBlond (1978) and Friedrichs and Madsen (1992) point out that, in frictionally dominated embayments and estuaries the lowest order dynamics is characterized by a zero-inertia equation, namely, a balance between the pressure gradient force and the bottom friction force. The zero-inertia equation also provides insight into the properties of higher-order harmonics via identification of compact approximate solutions and governing nondimensional parameters. A distortion parameter (γ) is thus derived to relate bottom friction, which is quantified as the ratio of tidal amplitude to mean water depth ratio (a/h_0), to intertidal storage (Friedrichs and Madsen, 1992):

$$\gamma = 5a/3h_0 - \Delta b/b_0 \tag{1}$$

where a is the amplitude of tidal elevation, h_0 is the average channel depth, and b_0 is the average channel width. $\Delta b = b - b_c$ where b is the total embayment width (including tidal flats or salt marshes), and b_c is the channel width at low water. The ratio of intertidal storage volume (V_i) to the channel volume (V_c) is parameterized by $\Delta b/b_0$. This equation shows the competing effect between frictional distortion (a/h_0) and intertidal storage ($\Delta b/b_0$), and predicts that tidal asymmetry is more sensitive to channel depth than to intertidal storage by a factor of 5/3. Friedrichs and Madsen (1992) show that flood dominance results when time variations in channel depth become more important than time variation in channel width ($\gamma > 0$); otherwise ($\gamma < 0$), ebb dominance results, as signified by increasingly large values of $\Delta b/b$.

Okatee Creek is a strongly dissipative tidal creek since tidal currents are greatly attenuated between station D and station OC-M (Table 2). Thus, the FVCOM experiments are a good candidate to examine the predictions of Eq. (1). For example in experiment OCE1, the intertidal storage parameter ($\Delta b/b_0$) is of order 10 near both stations which is significantly larger than the ratio of tidal amplitude to mean water depth which is of order 1. Hence, $\gamma < -8$, suggesting that the large intertidal storage area in the creek can cause stronger ebb currents that is confirmed by the FVCOM calculation (Fig. 6). In experiments OCE2 and OCE3, the intertidal storage parameters ($\Delta b/b_0$) are both approximately zero due to removal of the salt marsh zone and the increase in water depth. As a result the distortion parameter γ is a little greater than zero, which suggests a weak flood dominance or a less tendency to distort

the tide either way. This conclusion is also consistent with model prediction shown in Fig. 7a,b.

To further test the validity of the zero-inertia theory, time series of the terms in the vertically averaged momentum equations are plotted in Fig. 8. The vertically averaged momentum equations with constant density are (Chen et al., 2003):

$$\frac{\partial \overline{U}D}{\partial t} = -\frac{\partial \overline{U}\,\overline{U}D}{\partial x} - \frac{\partial \overline{U}\,\overline{V}D}{\partial y} + f\overline{V}D - gD\frac{\partial \xi}{\partial x} - \frac{\tau_{bx}}{\rho_0} + D\tilde{F}_x + G_x \tag{2}$$

$$\underbrace{\frac{\partial \overline{V}D}{\partial t}}_{\text{DDT}} = -\underbrace{\frac{\partial \overline{U}\,\overline{V}D}{\partial x} - \frac{\partial \overline{V}\,\overline{V}D}{\partial y}}_{\text{ADV}} - \underbrace{f\overline{U}D}_{\text{COR}} - \underbrace{gD\frac{\partial \xi}{\partial y}}_{\text{DP}} - \underbrace{\frac{\tau_{by}}{\rho_0}}_{\text{FRIC}} + \underbrace{D\tilde{F}_y}_{\text{VIS}} + \underbrace{G_y}_{\text{AV2D}} \tag{3}$$

where all variables are conventional and the overbar denotes vertical integration. In particular,

$$G_x = \frac{\partial \overline{U}\,\overline{U}D}{\partial x} + \frac{\partial \overline{U}\,\overline{V}D}{\partial y} - D\tilde{F}_x - \left[\frac{\partial \overline{U}\,\overline{U}D}{\partial x} + \frac{\partial \overline{U}\,\overline{V}D}{\partial y} - D\overline{F}_x\right]$$

$$D\tilde{F}_x = \frac{\partial}{\partial x}\left[2\overline{A}_m H\frac{\partial \overline{U}}{\partial x}\right] + \frac{\partial}{\partial y}\left[\overline{A}_m H\left(\frac{\partial \overline{U}}{\partial y} + \frac{\partial \overline{V}}{\partial x}\right)\right] \tag{4}$$

$$D\overline{F}_x = \frac{\partial}{\partial x}\overline{2A_m H\frac{\partial U}{\partial x}} + \frac{\partial}{\partial y}\overline{A_m H\left(\frac{\partial U}{\partial y} + \frac{\partial V}{\partial x}\right)}$$

The formulae for G_y, $D\tilde{F}_y$, and $D\overline{F}_y$ are similar.

The terms from left to right in Eqs. (2) and (3) are local inertia (DDT), advective inertia (ADV), Coriolis force (COR), barotropic pressure gradient (DP), bottom friction (FRIC), 2-D horizontal viscosity (VIS), and the difference between nonlinear terms of vertically-averaged 2-D variables

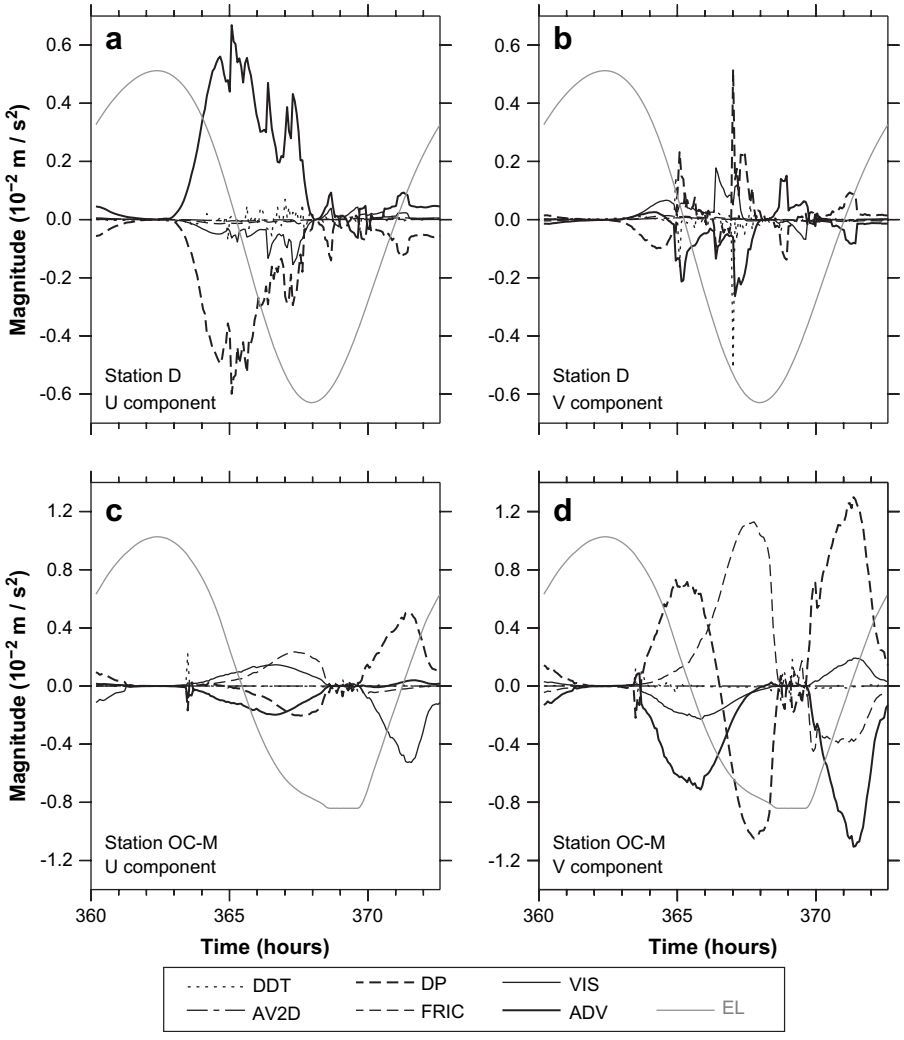

Fig. 8. Time series of vertically averaged terms in the 2-D momentum equations (Eqs. (2) and (3)). DDT represents the local inertia, ADV the advective inertia, DP the barotropic pressure gradient, FRIC the bottom friction, VIS the horizontal viscosity, and AV2D difference between 2-D and 3-D nonlinear terms. EL is the water surface elevation, which illustrates the tidal cycle. The Coriolis force (COR) term is always smaller and not shown. (a) Terms in the U-momentum equation for station D, (b) terms in the V-momentum equation for station D, (c) terms in the U-momentum equation for station OC-M, (d) terms in the V-momentum equation for station OC-M.

and vertical integration of 3-D variables (AV2D). Fig. 8 shows the time series of these terms in the last tidal cycle of experiment OCE1. At station D three terms dominate (Fig. 8a,b): the barotropic pressure gradient (DP), the advective inertia (ADV), and, to a less degree, the horizontal viscosity (VIS). Other terms, including the bottom friction (FRIC), are relatively small at this station. The importance of nonlinear advection in comparison to bottom friction at station D may be attributed to the fine grid spacing used in this application (about 20 m in the river channel) which allows larger lateral velocity shear compared to the coarse resolution model. Hence, the advective inertia (ADV) becomes increasingly dominant in horizontal momentum balance. Another salient feature at station D is that all the terms are smaller during rising tide than during falling tide. This is obviously related to the ebb dominance in the creek (Fig. 6) in which the maximum ebb currents are much larger than the maximum flood currents.

Due to the north–south orientation of the creek channel near station OC-M (Fig. 4), terms in the U momentum equation (Fig. 8c) for this station are much smaller than those in the V momentum equation (Fig. 8d). From Fig. 8d it is seen that the main momentum balance at station OC-M during ebbing tide is among the barotropic pressure gradient (DP), the bottom friction (FRIC), the advective inertia (ADV), and the horizontal viscosity (VIS), with the first two dominating when it is close to low water time. During rising tide, the dominating balance is between the barotropic pressure gradient (DP) and the advective inertia (ADV) with the other two terms (FRIC and VIS) also contributing. Hence, our numerical experiments suggest that bottom friction does not dominate advective inertia during the entire tidal period. There are periods in which terms related to lateral shear of the along-estuary velocity (i.e., the advective inertia and the horizontal viscosity) can be at least as important as the bottom friction term. This is consistent with experiment OCE4 (neglecting horizontal advection term) and OCE5 (linear bottom friction formulation) in that changes in these terms significantly alter the major balance in the momentum equations and thus change the asymmetric pattern of tidal fields. Therefore, our numerical experiments demonstrate that the zero-inertia assumption is not valid in Okatee Creek, nevertheless, the ebb dominance still prevails due to the existence of large areas of salt marsh.

The other type of tidal asymmetry, where the timing of the maximum ebb and flood currents is shifted closer to LWS, has also been found in other studies of shallow tidal creeks with large intertidal area (Postma, 1961; Dronkers, 1986; French and Stoddart, 1992; Blanton et al., 2002). It is believed that the time shift occurs when the river channel is surrounded by tidal flats which are covered soon after LWS. As pointed out by Dronkers (1986), when the tide spills into the intertidal storage area soon after LWS, the rate of water level increase slows, while the rising tide farther seaward continues unabated. This creates a strong upstream pressure gradient and a rapid acceleration to maximum flood shortly after LWS. Once the storage area is fully flooded, the pressure gradient diminishes and the current decelerates toward the point of HWS. The process reverses when the intertidal area drains. There is initially a slow acceleration in seaward pressure gradient and ebb current, which reach their maximums relatively close to the time of LWS.

Our base experiment (OCE1) shows that the maximum ebb and flood currents are shifted closer to LWS at the upstream station OC-M, which is consistent with the observations. Horizontal momentum analysis reveals that the maximum values of pressure gradient forcing (DP) do occur much closer to the LWS time at this station (Fig. 8d). However, FVCOM experiments fail to reproduce the observed time shift at station D. We believe that this may be attributed to the inaccurate bottom topography used in the model. Comparison of the FVCOM predicted hypsometric curve with the observation at station D (Fig. 9), the discrepancy is obvious near the time of LWS, which suggests that the numerical model has a steeper river channel wall and a wider channel breadth than its real world counterpart. This indicates that the interpolation process in generating model topographic data from DEM alters the nonlinear hypsometric curve to some degree and subsequently it changes the characteristics of asymmetric tidal field in the model.

The FVCOM experiments in Okatee Creek suggest that inclusion of the intertidal zone can significantly increase the simulated tidal current magnitude (OCE1 versus OCE2). We believe that this can be understood in view of volume conservation. As pointed out in Section 5, the amplitude of the tidal elevation is similar in the two experiments. Therefore, the experiment including the intertidal zone (OCE1) has to allow more water volume to flood in and drain out during an M_2 cycle than in the experiment where there is no intertidal zone (OCE2). Volume conservation requires larger tidal currents to allow the larger volume of water from the salt marshes to pass through the channel during each tidal cycle.

The simulation accuracy of the M_4 constituent is lower than that of the M_2 in experiment OCE1. Inaccurate bottom topography as inferred above is one of the reasons. The uncertainty in the bottom drag coefficient is another possible reason. In our numerical experiments a simple scheme is implemented

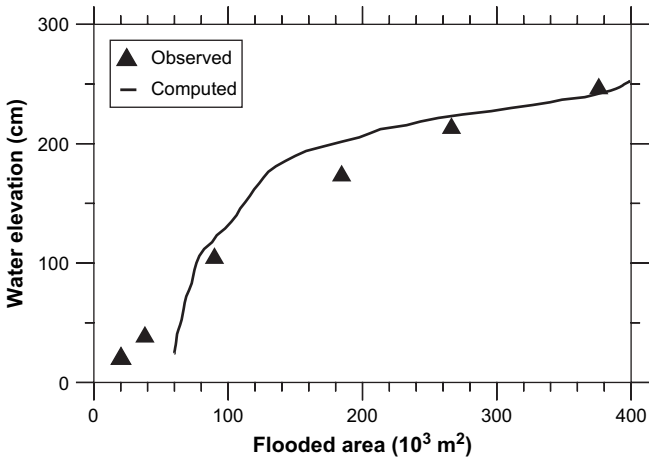

Fig. 9. Comparison between FVCOM-computed and -observed water level height and flooded area in Okatee Creek.

in which different constant drag coefficients are specified in the river channel and in the salt marsh zone respectively. We do not attempt to make this parameter truly space dependent, because doing so requires artificial adjustment of the parameter value without much physical or observational justification. However, from the many experiments conducted in which various bottom friction coefficient values are tested, it does show that the M_4 phase difference can be as large as 60–70°G from experiment OCE1. The bottom drag coefficients used in OCE1 are determined from best fit of harmonic constants between the model prediction and the observations. Similarly, the horizontal viscosity may also affect the calculated harmonic constants. In this study we do not attempt to tune this parameter and its value is set to the smallest possible one to make simulation stable.

Other factors responsible for model-data difference include: (1) wind effect, which may give rise to noise in the observed M_4 current due to overtide generation through wind and tide nonlinear interaction (Davies and Lawrence, 1994); (2) only two tidal constituents (M_2 and M_4) are considered in the simulations and, as a result, the influence of the neap–spring cycle is neglected; (3) short duration of current measurement at station D that introduces a relatively large error in observed harmonic constants. From the above considerations it is seen that the simulation of shallow water tides is a challenging task. When evaluating model performance in this study, we put more emphasis on the qualitative patterns of tidal asymmetry (i.e., flood/ebb dominance and timing of maximum ebb/flood current) than on overtide harmonic constants.

Summary

Observations show that the tidal currents in Okatee Creek are distorted from the sinusoidal form of their astronomical forcing, signifying a transfer of energy from M_2 to M_4. The main consequence of the overtide generation is to make ebb currents stronger than the flood currents. In addition, the maximum ebb and flood currents occur closer to the LWS time.

A 3-D numerical model, FVCOM, which utilizes a triangular horizontal grid to better fit the sinuous estuarine channel structure and boundary geometry, is applied to study tidal wave propagation and deformation in Okatee Creek. Model experiment results show that FVCOM provides an acceptable simulation of tidal elevations and currents. The qualitative pattern of tidal asymmetry is also reproduced. However, there are relatively large differences ($\sim$20°G) in the overtide phase between model prediction and the observation.

A set of numerical experiments are performed to test model sensitivity and to identify key nonlinear processes that generate the M_4 overtide. The experimental results suggest that the generation of the M_4 constituent is a result of nonlinear interaction of tidal currents with irregular creek geometry and bottom topography. Consistent with the classical view, the large volume of intertidal storage is the major reason for ebb dominance in Okatee Creek. However, the zero-inertia assumption is not always valid. In addition to the pressure gradient force and the bottom friction, advective inertia and horizontal viscosity are also important components in the horizontal momentum balance due to increased lateral velocity shear. The timing of the maximum ebb and flood currents occurring closer to LWS is probably related to the river channel morphology that is surrounded by salt marshes covered soon after LWS. Numerical experiments further reveal that exclusion of the flooding-drying process over the intertidal zone has little effect on the amplitude of M_2 and M_4 elevations. However, it severely underestimates both tidal currents and, thus, makes the tidal asymmetry less prominent.

Acknowledgements

We gratefully acknowledge the work of Dr Adelaide Ferreira (Guia Marine Laboratory, University of Lisbon) for calculation of the hypsometric curves from the aerial images and her assistance in producing the digital elevation model used to simulate the intertidal areas. We also gratefully thank David Stuebe (University of Massachusetts Dartmouth) for proofreading the manuscript and providing many suggestions. Constructive comments from two anonymous reviewers are greatly appreciated as well. This research was supported mainly by the NOAA Land Use – Coastal Ecosystem Study (LU-CES) Program funded through the South Carolina Sea Grant Consortium under grant number NA960PO113 and the Georgia Sea Grant College Program under grant number NA26RG0373. We also acknowledge the support of the Luso-American Foundation for funding the participation of F. Andrade in this project.

References

Aldridge, J.N., 1997. Hydrodynamic model predictions of tidal asymmetry and observed sediment transport paths in Morecambe Bay. Estuarine, Coastal and Shelf Science 44, 39–56.

Blanton, J.O., Andrade, F.A., 2001. Distortion of tidal currents and the lateral transfer of salt in a shallow coastal plain estuary (O Estuario do Mira, Portugal). Estuaries 24, 467–480.

Blanton, J.O., Lin, G., Elston, S.A., 2002. Tidal current asymmetry in shallow estuaries and tidal creeks. Continental Shelf Research 22, 1731–1743.

Blanton, J.O., Andrade, F., Adelaide Ferreira, M., 2006. The relationship of hydrodynamics and morphology in tidal-creek and salt-marsh systems in South Carolina and Georgia. In: Kleppel, G.S., DeVoe, M.R., Rawson Jr., M.V. (Eds.), Implications of Changing Land Use Patterns to Coastal Ecosystems. Springer-Verlag, New York, pp. 93–107.

Chen, C., Liu, H., Beardsley, R.C., 2003. An unstructured grid, finite-volume, three-dimensional, primitive equation ocean model: application to coastal ocean and estuaries. Journal of Atmospheric and Oceanic Technology 20, 159–186.

Chen, C., Beardsley, R.C., Cowles, G., 2004. An unstructured grid, finite-volume coastal ocean model FVCOM user manual. School for Marine Science and Technology. University of Massachusetts Dartmouth, New Bedford.

Chen, C., Huang, H., Blanton, J.O., Li, C., Andrade, F.A., submitted for Publication. Tidal-induced flushing process over the estuarine–tidal creek–salt marsh complex of the Okatee/Colleton River in South Carolina. Estuaries and Coasts (In Review).

Chen, C., Huang, H., Beardsley, R.C., Liu, H., Xu, Q., Cowles, G., 2007. A finite-volume numerical approach for coastal ocean circulation studies: comparisons with the finite-difference models. Journal of Geophysical Research 112, C03018, doi:10.1029/2006JC003485.

Davies, A.M., Lawrence, J., 1994. A three-dimensional model of the M_4 tide in the Irish Sea: the importance of open boundary conditions and influence of wind. Journal of Geophysical Research 99, 16197–16227.

Dronkers, J., 1986. Tidal asymmetry and estuarine morphology. Netherlands Journal of Sea Research 20, 117–131.

French, J.R., Stoddart, D.R., 1992. Hydrodynamics of salt marsh creek systems: implications for marsh morphological development and material exchange. Earth Surface Processes and Landforms 17, 235–252.

Friedrichs, C.T., Aubrey, D.G., 1988. Non-linear tidal distortion in shallow well-mixed estuaries: a synthesis. Estuarine, Coastal and Shelf Science 27, 521–545.

Friedrichs, C.T., Madsen, O.S., 1992. Non-linear diffusion of the tidal signal in frictionally dominated embayments. Journal of Geophysical Research 97, 5637–5650.

Friedrichs, C.T., Aubrey, D.G., 1994. Tidal propagation in strongly convergent channels. Journal of Geophysical Research 99, 3321–3336.

Galperin, B., Kantha, L.H., Hassid, S., Rosati, A., 1988. A quasi-equilibrium turbulent energy model for geophysical flows. Journal of Atmospheric Science 45, 55–62.

Jay, D., 1991. Green's law revisited: tidal long wave propagation in channels with strong topography. Journal of Geophysical Research 96, 20585–20598.

Lanzoni, S., Seminara, G., 1998. On tide propagation in convergent estuaries. Journal Geophysical Research 103, 30793–30812.

LeBlond, P.H., 1978. On tidal propagation in shallow rivers. Journal of Geophysical Research 83, 4717–4721.

Mellor, G.L., Yamada, T., 1982. Development of a turbulence closure model for geophysical fluid problem. Review or Geophysics and Space Physics 20, 851–875.

Nepf, H.M., Vivoni, E.R., 2000. Flow structure in depth-limited, vegetated flow. Journal of Geophysical Research 105, 28547–28557.

Parker, B.B., 1991. The relative importance of the various non-linear mechanisms in a wide range of tidal interactions (review). In: Parker, B.B. (Ed.), Tidal Hydrodynamics. John Wiley, New York, pp. 237–268.

Pawlowicz, R., Beardsley, R.C., Lentz, S., 2002. Classical tidal harmonic analysis including error estimates in MATLAB using T_TIDE. Computers and Geosciences 28, 929–937.

Postma, H., 1961. Transport and accumulation of suspended matter in the Dutch Wadden Sea. Netherlands Journal of Sea Research 1, 148–190.

Shetye, S.R., Gouveia, A.D., 1992. On the role of geometry of cross-section in generating flood-dominance in shallow estuaries. Estuarine, Coastal and Shelf Science 35, 113–126.

Smagorinsky, J., 1963. General circulation experiments with the primitive equations, I. The basic experiment. Monthly Weather Review 91, 99–164.

South Carolina Sea Grant Consortium, 2005. South Atlantic Bight Land Use-Coastal Ecosystem Study (LU-CES) Phase II Final Progress Report, 273 p. (unpublished).

Speer, P.E., Aubrey, D.G., 1985. A study of non-linear tidal propagation in shallow inlet/estuarine systems, Part II: theory. Estuarine, Coastal and Shelf Science 21, 207–224.

Speer, P.E., Aubrey, D.G., Friedrichs, C.T., 1991. Nonlinear hydrodynamics of shallow tidal inlet/bay systems. In: Parker, B.B. (Ed.), Tidal Hydrodynamics. John Wiley, New York, pp. 321–339.

Verduin, J.J., Backhaus, J.O., 2000. Dynamics of plant-flow interactions for the seagrass Amphibolis Antarctica: field observations and model simulations. Estuarine, Coastal and Shelf Science 50, 185–204.

Zheng, L., Chen, C., Liu, H., 2003. A modeling study of the Satilla River Estuary, Georgia. I: flooding-drying process and water exchange over the salt marsh–estuary–shelf complex. Estuaries 26, 651–669.